Journal of Biomedical Optics

SPIEDigitalLibrary.org/jbo

Confocal Raman microscopic investigation of the effectiveness of penetration enhancers for procaine delivery to the skin

Dominique Lunter
Rolf Daniels

SPIE

Confocal Raman microscopic investigation of the effectiveness of penetration enhancers for procaine delivery to the skin

Dominique Lunter* **and Rolf Daniels**
Eberhard Karls University of Tuebingen, Pharmaceutical Technology, Auf der Morgenstelle 8, 72076 Tuebingen, Germany

Abstract. A methodology that employs confocal Raman microscopy (CRM) on *ex vivo* skin samples is proposed for the investigation of drug content and distribution in the skin. To this end, the influence of the penetration enhancers propylene glycol and polyoxyethylene-23-lauryl ether on the penetration and permeation of procaine as a model substance was investigated. The drug content of skin samples that had been incubated with semisolid formulations containing one of these enhancers was examined after skin segmentation. The experiments showed that propylene glycol did not affect the procaine content that was delivered to the skin, whereas polyoxyethylene-23-lauryl ether led to higher procaine contents and deeper penetration. Neither substance was found to influence the permeation rate of procaine. It is thereby shown that CRM can provide additional information on drug penetration and permeation. Furthermore, the method was found to enhance the depth from which Raman spectra can be collected and to improve the depth resolution compared to previously proposed methods. [DOI: 10.1117/1.JBO.19.12.126015]

Keywords: confocal Raman microscopy; chemical imaging; skin; penetration enhancer; procaine.

Paper 140397RR received Jun. 22, 2014; accepted for publication Nov. 18, 2014; published online Dec. 24, 2014.

1 Introduction

The skin is the largest organ of the human body. It not only protects us from dehydration but also effectively inhibits the intrusion of harmful substances, microbes, parasites, and viruses. The skin can be divided into three main tissues: the epidermis, the dermis, and the hypodermis. The outermost layer of the epidermis is represented by the stratum corneum, which consists of flattened keratinocytes in a lipid matrix.[1] This lipid matrix is mainly composed of ceramides, free fatty acids, and cholesterol that form a highly ordered structure which exhibits excellent barrier function.[2] Despite its efficacy as a barrier, the skin is frequently used for the administration of drugs. Cutaneously applied drugs may be intended to be delivered dermally or transdermally, depending on their target structure. The rate and extent to which a drug penetrates and permeates the skin depends on its ability to penetrate the stratum corneum. This is, in turn, determined by the physicochemical properties of the drug molecule, particularly its lipophilicity and molecular weight.[3,4] Furthermore, the formulation in which the drug is applied to the skin affects the drug's penetration and permeation behavior. The concentration of the drug in the vehicle, the partition coefficient between the vehicle and the skin as well as the presence of penetration enhancers are among the factors that determine these characteristics.[5,6] Penetration enhancers may increase the partitioning of the drug into the skin, accelerate its diffusion through the skin and/or increase the solubility of the drug in the skin.[6] The mechanisms of action of penetration enhancers are numerous and include the disruption of the highly ordered structure of the lipids by intercalation in the alkyl chains and enhancement of the water content as well as alterations of the solubility of the drug in the skin.[5–7] Furthermore, specially designed drug delivery vehicles may be used to enhance drug penetration. To date, several different mechanisms have been proposed to explain the mode of action of nanocarriers. While some researchers state that they may penetrate the skin as such and release their contents into the skin,[8] others showed that such drug carriers cross the skin barrier intact and transport the active pharmaceutical ingredient (API) to the muscle bypassing the subcutaneous capillaries.[9] Those findings are contradicted by the results of spatially resolved diffusion measurements that show no colocation of a fluorescent probe and the vesicle compounds. This suggests a breakdown of the vesicles in the stratum corneum and a penetration enhancing effect of the vesicle compounds (comparable to that of oleic acid or other small molecules).[10]

To evaluate the effectiveness of the applied approach, the enhancement ratio is frequently calculated as the ratio of drug flux with enhancer and drug flux without enhancer.[11] This parameter can, consequently, only determine the influence of the penetration-enhancing principle on permeation through the skin; it does not assess the drug levels in the skin. If an intradermal action of the drug is intended, the evaluation of the drug concentration within the skin is pivotal as it correlates with the efficacy of the treatment. The different layers of the skin can be sampled by tape stripping (only assesses the stratum corneum) or (cryo-) segmentation of the skin (assesses all layers) and the drug content can subsequently be determined by appropriate analytical methods. In addition, optical methods such as attenuated total reflectance infrared microscopy (ATR-IR) and confocal laser scanning microscopy (CLSM) have been used to evaluate the penetration of xenobiotics into the skin.[12–14] Although both methods have been proven to be versatile tools, some disadvantages remain. ATR-IR exhibits a rather

*Address all correspondence to: Dominique Lunter, E-mail: dominique.lunter@uni-tuebingen.de

0091-3286/2014/$25.00 © 2014 SPIE

low spatial resolution of 10 to 13 μm and can, therefore, only give averaged spectra of the sampled area.[13] CLSM relies on either the fluorescence of the applied substance or the use of fluorescent labels.[12] These labels are often significantly larger than the penetrating substance itself and may bias the results. In the recent past, confocal Raman microscopy (CRM) has emerged as a promising method for the label-free imaging of the drug distribution in skin. In CRM, the chemical composition of a sample can be mapped at microscale resolution, and the relative distribution of the substances contained therein can be visualized. CRM has already been used to assess the composition of the skin,[15–17] the water content and distribution of the natural moisturizing factor,[18–20] and the distribution or penetration depth of various chemicals[14,21–32] as well as the effects of chemical and mechanical stress on the skin.[33,34] The above-mentioned studies proved that the detection of chemicals in the skin is possible, but some of the investigations were carried out using saturated solutions of model drugs;[23,24] others used substances that are not pharmaceutical actives but have been selected as optimal model substances with regard to their detectability by CRM.[20–22,29,30,35] By contrast, we used an API that targets the pain conducting fibers in the epidermis and in a concentration that was close to the therapeutically used concentration. Furthermore, we applied the API in a semisolid formulation and addressed the pharmaceutically relevant question of penetration enhancement. Here, we focused on the evaluation of the distribution of the API in the skin in particular. Procaine, a local anesthetic, was selected as a model substance. Procaine does not penetrate the skin as readily as its analog lidocaine. This is correlated to the partition coefficient ($k_{p(octanol/water)}$) of procaine, which is more than three times lower than that of lidocaine [($k_{p(octanol/water)}$) of procaine: 100; $k_{p(octanol/water)}$ of lidocaine: 366].[6,36] These poor penetration properties make it an ideal substance for studying the effectiveness of penetration enhancers, although it is not used dermally for the same reason. We chose propylene glycol and polyoxyethylene-23-lauryl ether (POE-23-lauryl ether) as penetration enhancers. Propylene glycol was chosen as it is known to enhance the penetration and/or permeation of a variety of drugs and is frequently used in dermal preparations (for example, see Refs. 37–40). POE-23-lauryl ether was chosen as Shin et al. showed that it enhanced the penetration of local anesthetics.[41] In their study, they assessed the effectiveness of the penetration enhancers by calculating the enhancement ratio. As outlined above, this does not assess the drug levels in the skin or the distribution of the drug in the skin. To characterize these parameters, we investigated skin samples by CRM. In contrast to the methods proposed so far for CRM investigations of skin, we employed sagittal cuts of samples of pig ear skin instead of tracking ingredients in the skin using virtual cross-sections that scan the sample from top to bottom (from the stratum corneum downward). This approach was used to circumvent the issues of decreased depth resolution and increased signal attenuation, which are a function of increasing depth,[42] and enabled us to evaluate the drug content and distribution in relation to the skin microstructure.

Consequently, the aim of the study was to investigate the distribution of the API in *ex vivo* cross-sections of skin by CRM. Furthermore, the influence of two penetration enhancers on the dermal delivery was investigated to show that the methodology is sensitive to differences in the API content in the skin on a scale that would be expected in dermal delivery. The outcome of the CRM study was compared to the results of the conventional methodology in which the enhancement ratio is calculated on the basis of the permeation rates.

2 Materials and Methods

2.1 *Materials*

Procaine HCl (Ceasar & Loretz GmbH, D-Hilden), hydroxypropyl methylcellulose (HPMC, Shin Etsu Chemical Co. Ltd., J-Tokyo), polyoxyethylene polyoxypropylene copolymer (Poloxamer 407, BASF SE, D-Ludwigshafen), polyoxyethylene-23-lauryl ether (POE-23-lauryl ether, Croda GmbH, D-Nettetal-Kaldenkirchen), propylene glycol (BASF SE, D-Ludwigshafen), tissue embedding medium NEG 50 (Thermo Scientific Inc., D-Langenselbold). Disodium hydrogen phosphate, potassium dihydrogen phosphate, sodium chloride and ethanol were Ph. Eur. grade. Pig ears were supplied by the Department of Experimental Medicine at the University of Tuebingen.

2.2 *Preparation of Semisolid Formulations*

HPMC-poloxamer gels were prepared according to the method published by Shin et al.[41] First, 1 g of procaine HCl was dissolved in water. For preparations containing penetration enhancers, 0.5 g of propylene glycol or 0.5 g of POE-23-lauryl ether was dissolved in the aqueous procaine HCl solution. Thereafter, 0.2 g of HPMC and 2 g of poloxamer 407 were dispersed in the solution by a magnetic stirrer. The preparations were stored at 4°C to 8°C overnight to ensure complete swelling of the polymers and were refrigerated until the day of the experiment. The compositions of the formulations are given in Table 1.

2.3 *Preparation of Dermatomed Pig Ear Skin*

Postauricular skin of female pigs of the german landrace was used for *in vitro* permeation and penetration experiments. The donor pigs were 15 to 30 weeks old and weighed 40 to 65 kg. Fresh pig ears were washed with isotonic saline. Postauricular skin was excised. Skin samples were cleaned of blood with isotonic saline and cotton swabs, patted dry with

Table 1 Composition of the semisolid formulations [g].

	HPMC	Poloxamer	Propylene glycol	POE-23-lauryl ether	Procaine HCl	water
Without enhancer	0.2	2.0	0	0	1.0	6.8
With propylene glycol	0.2	2.0	0.5	0	1.0	6.3
With POE-23-lauryl ether	0.2	2.0	0	0.5	1.0	6.3

tissue, wrapped in aluminum foil and stored at −30°C. On the day of the experiment, the skin was thawed at room temperature, cut into strips of ∼3 cm in width and fixed to a block of Styrofoam with pins. The skin was dermatomed to a thickness of 1 mm (Dermatom GA 630, Aesculap AG & Co. KG).

2.4 *Preparation of Diffusion Cells*

In vitro penetration and permeation tests were conducted using modified Franz diffusion cells (Gauer Glas, D-Püttlingen) with a receptor volume of 12 mL and a diffusion area of 2 cm^2. A 70:30 (m/m) mixture of phosphate-buffered saline (PBS) pH 7.4 (Ph. Eur. 7) and ethanol was used as the receptor fluid. The Franz diffusion cells were filled with degassed, prewarmed (32°C) receptor medium. Thereafter, the Franz diffusion cells were equipped with dermatomed pig ear skin (thickness: 1 mm, diameter: 25 mm) and donor compartments. The formulations were withdrawn from the refrigerator, and 0.5 mL of the formulation was applied to the skin surface. As the formulations contained poloxamer, they were fluid at low temperatures, and dosing could be conducted with a disposable 1-mL syringe. The viscosity of the formulations then increased rapidly upon application to the warm skin (32°C). The cells were capped with Parafilm to prevent the evaporation of water. The experiments were performed at 32°C and a stirring speed of 500 rpm.

2.5 *In Vitro Permeation Experiments*

Procaine was allowed to permeate the skin over a period of 38 h. In the permeation experiments, 1 mL aliquots were withdrawn after 14, 20, 23, and 38 h. The sample volume was replaced by fresh, prewarmed receptor medium. Samples were analyzed by HPLC. The experiments were performed in quintuplicate. The cumulative amount permeated per unit area was plotted against time, and the permeation rate was calculated as the slope of this graph (Fig. 8). The apparent partition coefficient (skin/vehicle) of procaine HCl was calculated using the following equation:[6]

$$K = \frac{J_{ss} h}{DC}, \tag{1}$$

where J_{ss} = steady-state flux (mg/cm^2/h), D = diffusion coefficient (cm^2/h), K = partition coefficient of the drug (skin/vehicle), c = concentration of the drug in the vehicle (mg/cm^3), and h = skin thickness (cm).

Permeation rates and apparent partition coefficients are given in Table 3.

2.6 *In Vitro Penetration Experiments*

In conventional penetration experiments, the incubated skin samples were withdrawn from the diffusion cells after 14 h. Residual formulation was removed from the skin with cotton swabs and PBS. Subsequently, the penetration area (1.5 cm in diameter) was punched out. The skin samples were patted dry with cotton swabs. The stratum corneum was removed by cyanoacrylate biopsies. It was found necessary to conduct five biopsies in order to remove the stratum disjunctum and the stratum compactum. For this, a small amount of cyanoacrylate glue was added to the skin surface and a glass slide was attached to it by gentle pressing for 90 s. Subsequently, the glass slide was torn away with one gentle move. This procedure was repeated four times. Then, the skin samples were frozen in liquid nitrogen. The skin samples were removed from the liquid nitrogen, embedded in tissue embedding medium, and fixed to the sample holder of a cryo microtome (HM 560 Cryo-Star; Thermo Fisher, D-Langenselbold) in such a way that the epidermis was free of tissue embedding medium and was oriented upwards. The skin was segmented according to a previously validated protocol. In the beginning, the skin was segmented in 50 μm slices. Incomplete cuts (usually one or two) as well as the first complete cut were assigned to the viable epidermis. The remaining skin was segmented into one cut of 50 μm and 9 cuts of 100 μm and was assigned to the dermis. The cuts were collected in centrifuge tubes (15 mL, VWR International GmbH, D-Darmstadt). The centrifuge tubes were weighed before and after addition of the skin cuts in order to determine the weight of the sampled skin. Thereafter, 2 mL of ethanol was added to the tubes. Similarly, the glass slides with the cyanoacrylate biopsies were inserted into centrifuge tubes (50 mL, VWR International GmbH, D-Darmstadt) and 40 mL of ethanol was added. The tubes were wrapped with parafilm™ to prevent the evaporation of ethanol. Procaine was extracted from the skin samples at room temperature over 15 h. Subsequently, 1 mL of the clear supernatant was sampled into HPLC vials. Procaine content was determined by HPLC. The procaine amount was normalized to the weight of the skin samples. For the stratum corneum, 3 mg was set as its weight as preliminary experiments had given this value. The results are given as procaine amount per milligram of tissue. The total amount of procaine within the skin was calculated as the sum of the procaine amount in stratum corneum, viable epidermis, and dermis. From the total amount of procaine in the skin, an enhancement ratio was calculated as the ratio of drug content with enhancer and drug content without enhancer. Experiments were made in quintuplicate.

2.7 *Sample Preparation for CRM Analysis of Incubated Pig Ear Skin*

In CRM-penetration experiments, the incubated skin samples were withdrawn from the diffusion cells after 14 h. Residual formulation was removed from the skin with cotton swabs and PBS. Subsequently, the penetration area (1.5 cm in diameter) was punched out. The skin samples were patted dry with cotton swabs and frozen in liquid nitrogen. The skin samples were removed from the liquid nitrogen, partially embedded in tissue embedding medium, and fixed to the sample holder of a cryomicrotome (HM 560 Cryo-Star; Thermo Fisher, D-Langenselbold). Cross-sections of 50 μm were cut as illustrated in Fig. 1. The skin was fixed in the sample holder such that no substances would be carried from the stratum corneum into deeper layers of the skin as a result of the cutting process. The cuts were transferred to glass slides and kept humid until analysis.

2.8 *CRM Analysis*

A confocal Raman setup was used to map the microstructure of the skin and distribution of procaine in relation within it. An alpha 500 CRM (WiTec GmbH, D-Ulm) equipped with a 532 nm laser and a 10× objective (NA 0.25) was used. The laser intensity was adjusted to its maximum power using a Silica sample, resulting in an intensity of 36 mW on the sample surface. All calculations were performed with the WiTec Project 2.10 integrated software (WiTec GmbH, D-Ulm).

In the beginning, a spectral data set of neat skin was analyzed with the goal to define a certain number of spectra that can

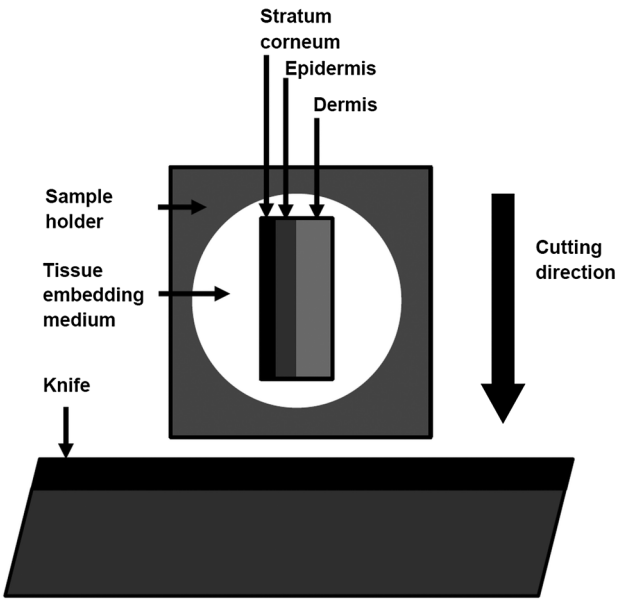

Fig. 1 Scheme of the experimental setup for cryosegmentation of the skin.

explain the spectral variances that occur as a result of skin depth. An area of 20×200 μm was mapped with 20×200 pixels (4000 spectra) with a lateral resolution of 1.3 μm, an integration time of 2 s, and a grating of 1800 g/mm, resulting in a spectral resolution of 1 cm^{-1}. The spectral range covered the "fingerprint region" between 720 and 1820 cm^{-1}. The scans were processed by cosmic ray removal and baseline correction. Subsequently, the spectra were subjected to a *k*-means cluster analysis. The whole spectral range (720 to 1820 cm^{-1}) was used for clustering. The Manhattan distance mode was used. Initially, two clusters were created. Clustering was repeated several times until the resulting spectra did not differ substantially from the input spectrum. Subsequently, four spectra which described all the variances in the spectra from the skin sample were identified.

For visualization of the procaine distribution in the skin, areas of 20×70 μm (20×70 pixels) were mapped with a lateral resolution of 1.3 μm, an integration time of 2 s, and a grating of 1800 g/mm, resulting in a spectral resolution of 1 cm^{-1}. The spectral range covered the "fingerprint region" between 720 and 1820 cm^{-1}. The scans were processed by cosmic ray removal and baseline correction. For the calculation of color-coded images, the four spectra that were extracted from neat skin by a *k*-means cluster analysis (see Figs. 2 and 3) and the ν (C=C) β (NH_2)-scissoring mode of procaine at 1600 to 1625 cm^{-1} was used. First, intensity maps for each skin spectrum and for procaine were generated by a least squares fit on the basis of Eq. (2).[43]

$$\vec{S} = \sum_{k=1}^{N} a_k \vec{B}_k, \tag{2}$$

where each raw material has its Raman spectrum $\vec{B}_k$ and a sample consists of N different raw materials that show a linear superposition $\vec{S}$. In this case, the weighting factor a_k which is proportional to the quantity of the raw material can be estimated. The weighting factors for the different raw materials are then displayed as intensity maps.[43] The four skin spectra and the peak obtained from the ν (C=C) β (NH_2)-scissoring mode of procaine were used to calculate the intensity maps for these five materials. Each material was assigned a color and the five intensity maps were merged to give a color coded image.

For a semiquantitative analysis of the procaine content in the skin samples, the procaine peak (1600 to 1625 cm^{-1}) was normalized to the δ (CH_2, CH_3) mode (1430 to 1490 cm^{-1}). Normalization is a standard procedure to overcome intersample intensity variations in biological samples. In skin samples, this is frequently performed by normalization to the "keratin signal," which refers to a peak located between 2910 and 2965 cm^{-1} resulting from the ν (CH_3) mode of proteins. The procedure was first described by Caspers et al.[20] (for example, see Refs. 20, 22, 24, 25, and 44). As we collected spectra in the range of 720 to 1820 cm^{-1}, the normalization was not performed on the ν (CH_3) mode but on the δ (CH_2, CH_3) mode. The rationale for this choice was that both peaks arise from the same bonds and the variations of the two peaks within the skin are similar (our comparison of the respective peak areas gave $r > 0.9$).[45] In all scans, an area could be detected in which the spectra had a high intensity. This area was identified as the stratum corneum compactum. To calculate the relative amount of procaine in the stratum corneum, we first drew a line perpendicular to the skin surface in the middle of the *x*-direction of the image scan. Subsequently, we extracted all spectra along this line. From these, we selected the spectrum with the highest intensity of the δ (CH_2, CH_3) mode (1430 to 1490 cm^{-1}). We calculated the relative procaine amount in the startum corneum as the ratio of the area under the procaine peak (1600 to 1625 cm^{-1}) and the area under the δ (CH_2, CH_3) mode (1430 to 1490 cm^{-1}) in this spectrum (see Fig. 10 for an illustration of the method.).

To calculate the relative procaine amount in the whole sample, all spectra of the image scan were used. From each spectrum, the areas under the procaine peak (1600 to 1625 cm^{-1}) and the areas under the δ (CH_2, CH_3) mode (1430 to 1490 cm^{-1}) were calculated and summed up. From the sum of the procaine peak areas and the sum of areas of the δ (CH_2, CH_3) mode, we calculated the relative procaine amount in the whole sample as the ratio of the sum of all areas under all procaine peaks (1600 to 1625 cm^{-1}) and all areas under all δ (CH_2, CH_3) peaks (1430 to 1490 cm^{-1}). By this procedure, we obtained one value for the procaine amount in the stratum corneum [C_{SC}(procaine)] and a second value for the procaine amount in the whole sample [C_{skin}(procaine)] for each formulation. To calculate the enhancement ratio, the C_{skin}(procaine) of the formulation with enhancer was divided by the C_{skin}(procaine) of the formulation without enhancer.

The penetration depth was calculated as the distance between the position in the stratum corneum at which the spectrum with the highest intensity of the δ (CH_2, CH_3) mode was detected and the position at which the procaine signal was below the limit of detection.

CRM analysis was performed on three independent skin samples per formulation and skin donor. The skin of three different donors was used, resulting in a total of 27 samples. The results obtained from one donor are given in Table 2 and Figs. 5–7. Similar results were observed with the other donors.

2.9 *Procaine Quantification*

Procaine was quantified using the LC-20A prominence HPLC system (Shimadzu, D-Duisburg). The HPLC column Nucleosil

100-5C 8 CC 125/4 (Macherey-Nagel, D-Dueren) was used in combination with the HPLC precolumn Nucleosil 100-5 C8CC 8/3 (Macherey-Nagel, D-Dueren). The column-oven temperature was set to 50°C. The eluent consisted of 40% methanol and 60% phosphoric acid, pH 3.0. The flow was set to 1.15 mL/ min. In the course of the experiment, 20 μL aliquots were injected, and the UV absorbance was measured at 220 nm. Procaine was eluted after ~4 min. The peak areas were used for the calculation of the procaine concentration. The calibration used for the samples from permeation experiments covered the range of 0.05 to 1.0 mg/mL. The limit of detection was calculated as 0.004 mg/mL, the limit of quantification as 0.012 mg/Ml, and the coefficient of determination as 0.999992 mg/mL.[46] The calibration used for the samples of epidermis and dermis from penetration experiments covered the range of 0.002 to 0.02 mg/mL. The limit of detection was calculated as 0.001 mg/mL, the limit of quantification as 0.002 mg/mL, and the coefficient of determination as 0.9993.[46] The calibration used for the samples of stratum corneum from penetration experiments covered the range of 0.0002 to 0.0016 mg/mL. The limit of detection was calculated as 0.00006 mg/mL, the limit of quantification as 0.00017 mg/mL, and the coefficient of determination as 0.9993.[46]

2.10 *Statistical Analysis*

The data were obtained from repeated measurements (permeation and penetration data: $n = 5$; Raman data: $n = 3$). The descriptive statistics calculated include the geometric mean as well as the highest and lowest individual values. When appropriate, the data were analyzed by the Wilcoxon–Mann–Whitney U test ($p < 0.05$). Data that are significantly different are marked with a superscript "a."

3 Results

3.1 *CRM Analysis of Procaine Penetration into Skin*

Figure 2 shows a microscopic image, a color-coded image obtained from a CRM analysis of postauricular porcine skin and the spectra that correspond to the spots indicated by crosses in the CRM image. The three strata—the stratum corneum, viable epidermis and dermis—can be clearly distinguished in the microscopic image. The results of the CRM analysis show that the intensity of the whole Raman spectrum and that of individual peaks varies within the skin. The most intense peaks correspond to aromatic amino acids (1004 cm^{-1}), the υ (C-C) mode of the lipid components (1000 to 1150 cm^{-1}), the δ (CH_2) and δ (CH) modes (1300 to 1350 cm^{-1}), the δ (CH_2) scissoring and δ (CH_3) modes (1430 to 1490 cm^{-1}) and the υ (C=O)-amide I mode (1640 to 1700 cm^{-1}).[33,34,47] The variation of the intensity of the whole spectrum is correlated to the optical density of the tissue, whereas variations in the intensity of single peaks are due to variations in the composition of the strata.[21] The intensity of the spectra is highest in the stratum corneum compactum, which is formed by five to six layers of densely packed corneocytes in a lipid matrix.[48] Prominent differences were observed in the spectral regions between 1000 and 1150 cm^{-1} and 1230 and 1370 cm^{-1}. The peaks at 1066 and 1130 cm^{-1} are, therefore, most prominent in the stratum corneum region, whereas the band at 1100 cm^{-1} is more pronounced in deeper layers of

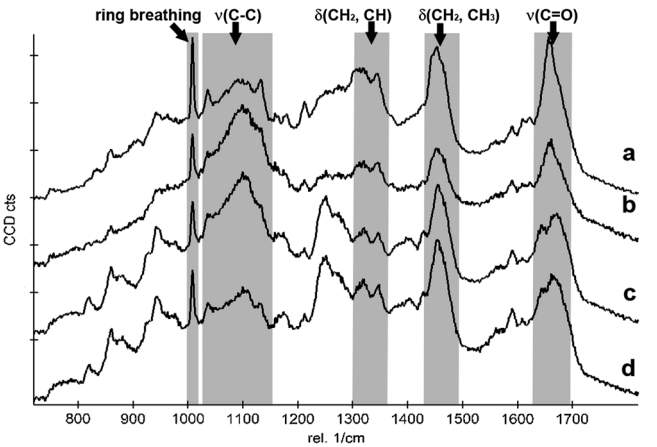

Fig. 3 Spectra extracted from Fig. 3(b) by *k*-means cluster analysis.

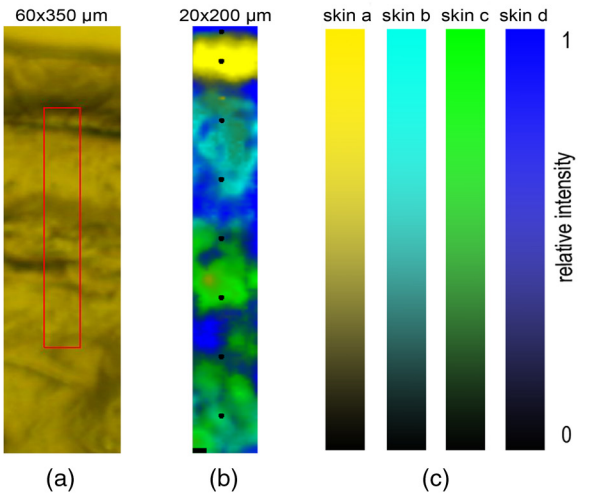

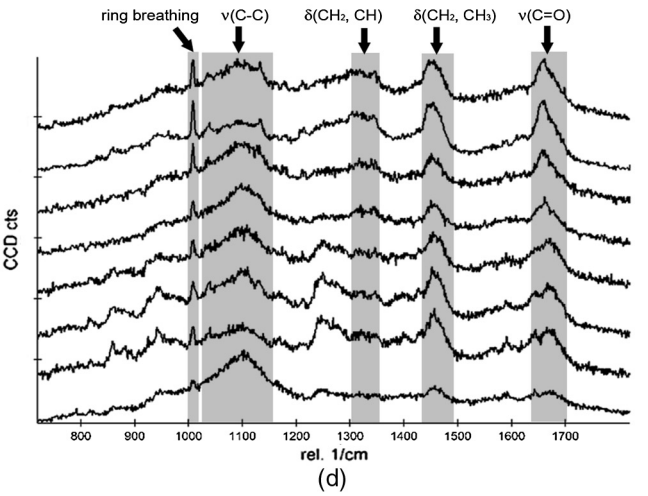

Fig. 2 Representative images of an *ex vivo* cross section of postauricular porcine skin. (a) microscopic image; the box indicates the area from which the Raman scan was made (b) color-coded CRM image (c) color scale bars (d) spectra extracted from the spots indicated in (b).

the skin.[16] The region between 1250 and 1350 cm^{-1} corresponds to the amide III band, which is influenced by the different conformational structures of the proteins.[15,34] The amide III band is more pronounced in deeper layers of the skin, i.e., in tissues that contain higher amounts of proteins. A more detailed discussion of the skin Raman spectra can be found in Refs. 15, 16, 21, 33, 34, and 47.

A *k*-means cluster analysis extracted four spectra that describe the observed spectral variations. The spectra are given in Fig. 3. Spectrum (a) dominates in the stratum corneum (the layer of the skin with the highest optical density) and is characteristic of highly ordered lipid structures. Spectrum (b) represents areas of the skin with a high content of lipids in the gauche conformation. Spectrum (c) shows a high lipid content but unordered lipid structures. Changes in the amide III band provide evidence of a change in the structure of the proteins. Spectrum (d) is influenced by the ordered structure of lipids and similar changes in the amide III band as in spectrum (c). These four spectra were used in the subsequent investigations.

Figure 4 compares the spectra of the ingredients of the formulations, procaine HCl, skin, and skin incubated with procaine HCl-containing formulations. The spectrum of procaine HCl shows several peaks in the sampled spectral region. The peak at 1600 to 1625 cm^{-1} which results from the ν (C═C)-mode and the β (NH_2)-scissoring mode[49] can also be found in the spectra of skin samples incubated with procaine HCl. This peak was used in further experiments for the evaluation of procaine content and distribution in the skin. No traces of the other ingredients of the formulations could be detected in the incubated skin (for spectra of skin incubated with placebo formulations, see Figs. 11–13).

Figure 5 shows a microscopic image and a color-coded image obtained from a CRM analysis of skin incubated with a semisolid preparation that contained procaine HCl. Spectra that were extracted along a line perpendicular to the skin surface are also shown. The exact locations from which the spectra were extracted are marked with crosses. The characteristic peak of procaine can be identified in the spectra of the skin sample. It is rather small compared to the peaks that correspond to the skin.

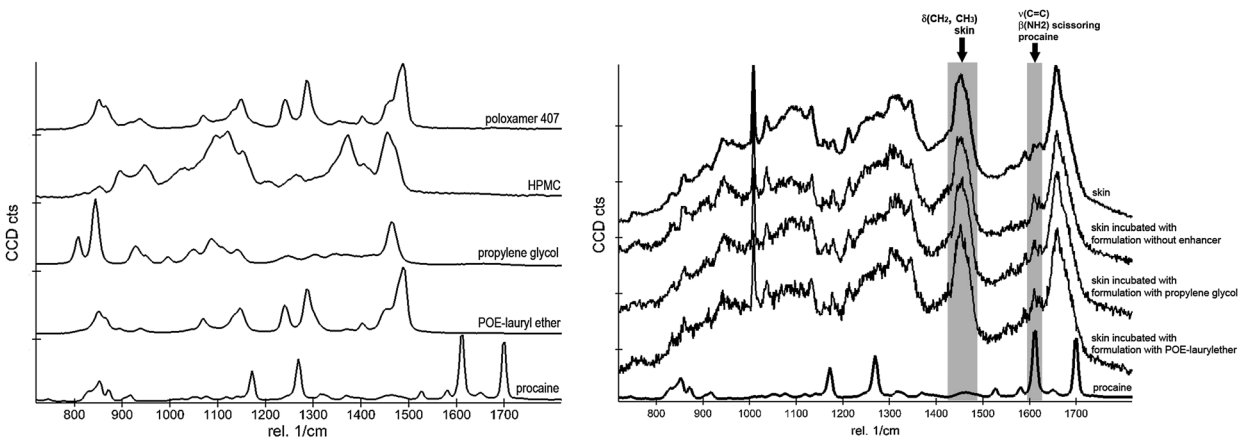

Fig. 4 Spectra of procaine HCl, the ingredients of the formulations (a) and of skin that was incubated with the formulations (b).

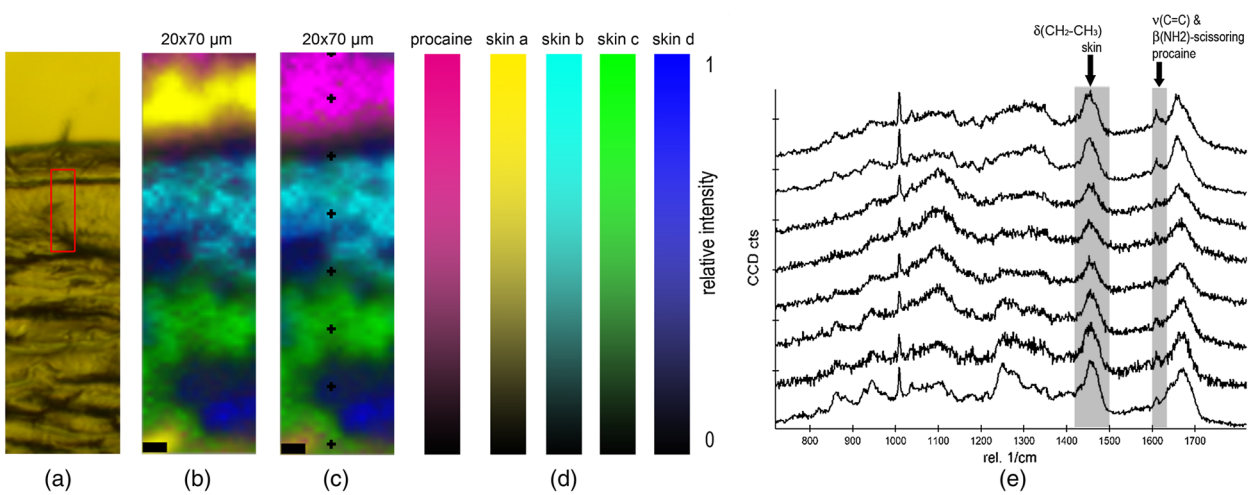

Fig. 5 Representative images of *ex vivo* cross-sections of skin incubated with a formulation that contained procaine HCl (a) microscopic image; the box indicates the area from which the Raman scan was made (b) color-coded CRM image [top layer: skin(b)] (c) color-coded CRM image (top layer: procaine) (d) color scale bars (e) spectra extracted from the spots indicated in (c).

Table 2 Normalized peak areas of the procaine peak (1600 to 1625 cm^{-1} [a. u.].

	In the stratum corneum				In the whole sample			
	Geometric mean	Max. value	Min. value	Enhancement ratio	Geometric mean	Max. value	Min. value	Enhancement ratio
Without enhancer	0.11	0.15	0.10		0.09	0.11	0.06	
With propylene glycol	0.11	0.12	0.10	1.0	0.08	0.11	0.05	0.9
With POE-23-lauryl ether	0.24	0.28	0.21	2.1	0.20	0.22	0.18	2.3

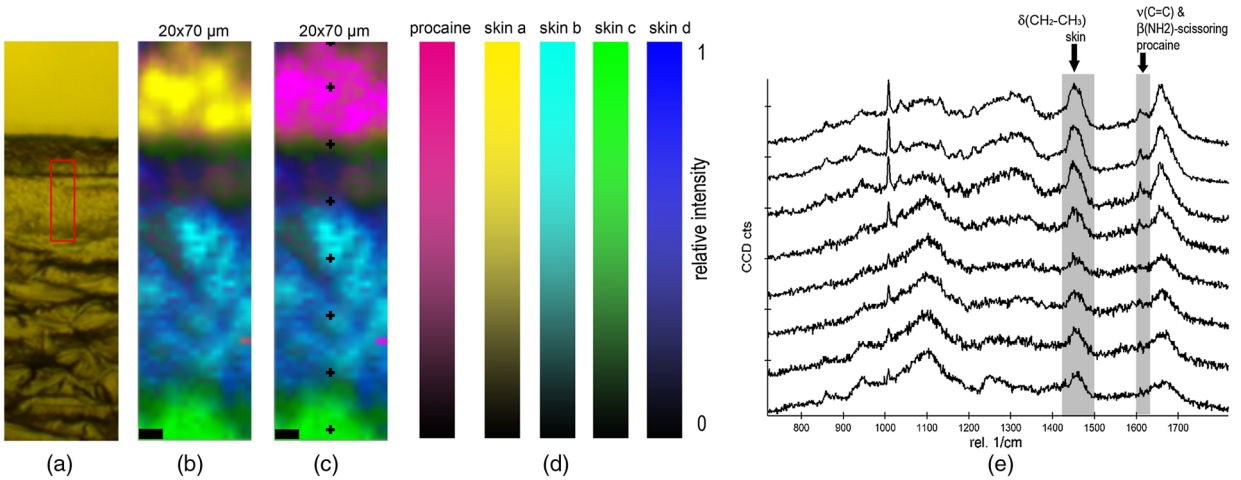

Fig. 6 Representative images of *ex vivo* cross sections of skin incubated with a formulation that contained procaine HCl and propylene glycol (a) microscopic image; the box indicates the area from which the Raman scan was made (b) color-coded CRM image [top layer: skin(b)] (c) color-coded CRM image (top layer: procaine) (d) color scale bars (d) spectra extracted from the spots indicated in (c).

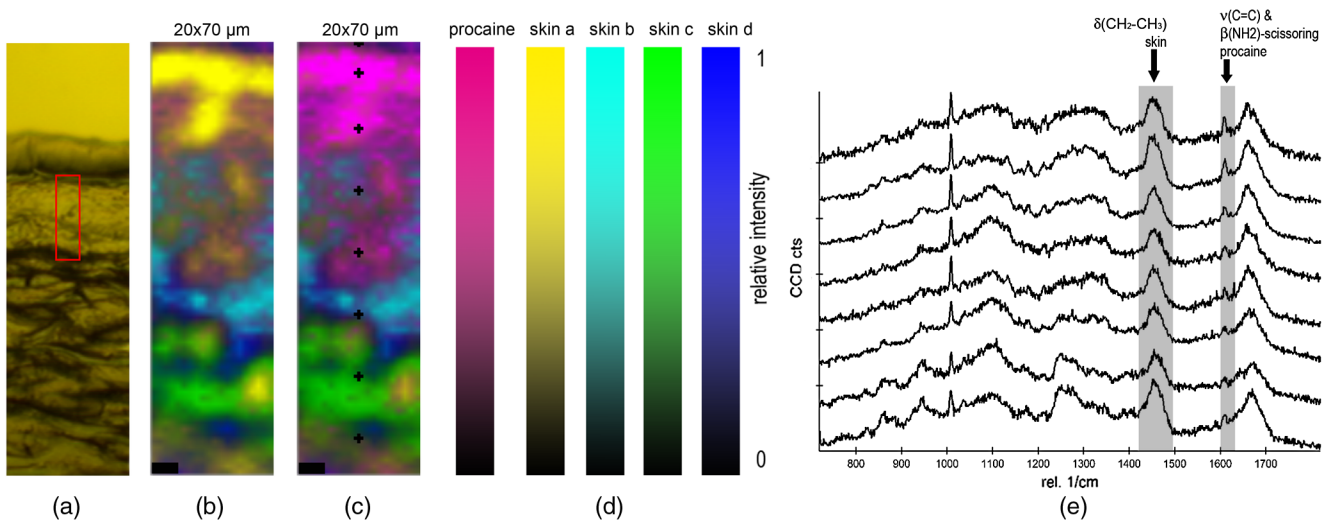

Fig. 7 Representative images of *ex vivo* cross sections of skin incubated with a formulation that contained procaine HCl and POE-23-lauryl ether (a) microscopic image; the box indicates the area from which the Raman scan was made (b) color-coded CRM image [top layer: skin(b)] (c) color-coded CRM image (top layer: procaine) (d) color scale bars (d) spectra extracted from the spots indicated in (c).

The highest procaine content (highest intensity of the procaine peak relative to the intensity of the δ (CH_2, CH_3) mode) can be found in the stratum corneum. Here, the normalized procaine intensity is 0.11 (Table 2). The overall procaine content decreases with increasing depth. Procaine could be detected to a depth of ~20 μm.

The results of penetration experiments with the formulations that contained either propylene glycol or POE-23-lauryl ether are shown in Figs. 6 and 7. After penetration from the vehicle that contained propylene glycol, a small procaine peak can be observed in the spectra. Again, the highest procaine content was found in the stratum corneum (normalized procaine intensity: 0.11). The intensity of the procaine peak decreases with increasing depth. Procaine was detected in the skin up to a depth of ~20 μm. Penetration experiments with the formulation that contained POE-23-lauryl ether reveal a different picture. The spectra that were extracted from the CRM image scan show an intense procaine peak. In the stratum corneum, the normalized procaine intensity is 0.24. The intensity of the procaine peak relative to the δ (CH_2, CH_3) mode decreases with increasing depth. Interestingly, the color-coded CRM image shows a higher procaine content in an area of high lipid content at a depth of 40 to 50 μm (dermis) than in the adjacent, more hydrated tissue. This behavior can be explained by the lipophilic nature of procaine. The CRM image shows that procaine was detected in the skin up to a depth of 60 μm. At this depth, the normalized procaine intensity is still 0.08.

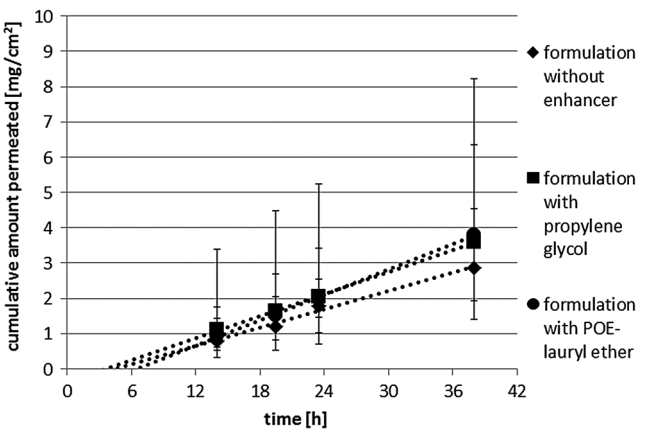

Fig. 8 Permeation of procaine through porcine skin.

3.2 *Analysis of Permeation of Procaine through Skin*

The permeation rate of procaine was determined to evaluate the effectiveness of the penetration enhancers to deliver procaine through the skin and to correlate the amount permeated to the results of the CRM analysis. Figure 8 compares the permeation of procaine from the three formulations, and Table 3 summarizes the relevant parameters. We found that the flux of procaine was 0.09 mg/cm^{2}h from the formulation without enhancers, 0.10 mg/cm^{2}h from the formulation with propylene glycol, and 0.12 mg/cm^{2}h from the formulation with POE-23-lauryl ether. The permeation rates as well as the total amounts permeated varied strongly from one skin sample to the other, which may be related to the generally low skin permeability of procaine. As a result, no significant difference ($p < 0.05$) could be found between the permeation rates from the three formulations.

The apparent partition coefficient of procaine HCl between the skin and the vehicle was also calculated. Interestingly, the variations in the partition coefficient were smaller than the variations in flux and the cumulative amount permeated. Partition coefficients of 0.26, 0.20 and 0.47 were obtained for the formulation without enhancer, the formulation with propylene glycol, and the formulation with POE-23-lauryl ether, respectively (see also Table 3). The statistical analysis revealed the partition coefficient of the formulation with POE-23-lauryl ether to be significantly higher than the partition coefficient of procaine when it permeated from the other two formulations.

3.3 *Analysis of Penetration of Procaine into the Skin*

Penetration experiments were carried out to compare the amount of API that was delivered to the different strata by the formulation without enhancer and the formulation with POE-23-lauryl ether. The formulation with propylene glycol was not examined as neither the CRM-measurements nor the permeation experiments had shown any effect of propylene glycol on the penetration or permeation of procaine. Results are given in Fig. 9 and Table 4. The total amount of procaine that was delivered from the formulation with POE-23-lauryl ether was found to be 2.6 times higher than from the formulation without enhancer. Looking at the different strata, it can clearly be seen that the predominant amount of procaine is located in the stratum corneum. For all three strata, the amount of procaine that was delivered from the formulation with

Table 3 Comparison of flux values and partition coefficients of procaine after permeation through excised pig ear skin.

	Flux (mg/cm^{2}h)			Enhancement ratio	Partition coefficient		
	Geometric mean	Max. value	Min. value		Geometric mean	Max. value	Min. value
Without enhancer	0.09	0.13	0.05		0.26	0.32	0.21
With propylene glycol	0.10	0.19	0.06	1.11	0.20	0.23	0.18
With POE-23-lauryl ether	0.12	0.13	0.09	1.33	0.47[a]	0.62	0.34

[a]Note: Values that are significantly different.

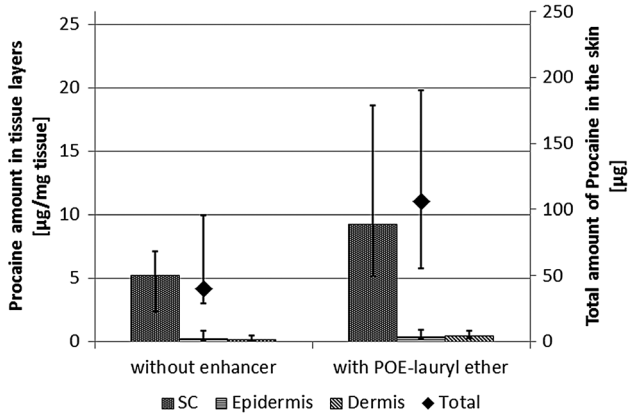

Fig. 9 Penetration of procaine into porcine skin.

Table 4 Results of the conventional *in vitro* penetration experiment.

	Total amount of procaine penetrated (μg)			
	Geometric mean	Max. value	Min. value	Enhancement ratio
Without enhancer	40	95	29	
With POE-23-lauryl ether	106	190	55	2.6

POE-23-lauryl ether is distinctly higher than that from the formulation without enhancer.

Together with the results of the permeation experiment, this leads to the conclusion that POE-23-lauryl ether will enhance the efficacy of procaine in the skin without enhancing the systemic absorption.

4 Discussion

A comparison of the CRM images and the corresponding spectra reveals that procaine is mainly located in the lipid-rich structures of the skin. The highest contents can be found in the stratum corneum. Significant amounts are also present in the lipid-rich regions in the deeper skin layers. By contrast, the amount of procaine in the adjacent, more hydrated tissue is rather small.

The CRM images show that the penetration depths that are achieved with the different vehicles increase in the following order: formulation with propylene glycol = formulation without enhancer > formulation with POE-23-lauryl ether. Comparison of the intensities of the characteristic procaine peak in the skin after incubation with or without enhancer proves that the corresponding peak area increases in the same order. This indicates that the concentration of procaine in the skin is not affected when it is delivered from a vehicle that contains propylene glycol and that the penetration is highest from a vehicle containing POE-23-lauryl ether. Likewise, the penetration depth and the amount of procaine in the whole sample are not affected by propylene glycol. By contrast, the area of the procaine peak in the stratum corneum is increased 2.1-fold when procaine penetrated from the vehicle with POE-23-lauryl ether compared to the peak after penetration from the vehicle without enhancer. It can, therefore, be concluded that a 2.1-fold higher amount of procaine is delivered to the stratum corneum when using POE-23-lauryl ether as a penetration enhancer. Furthermore, the penetration depth is greater from the vehicle containing POE-23-lauryl ether, and the procaine content in the viable epidermis is thus enhanced. The normalized procaine peaks at a depth of 60 μm prove this, as they are 0 for the formulation without enhancer and 0.08 for the formulation with POE-23-lauryl ether. This phenomenon is also reflected by the enhancement ratio of 2.3 calculated from the normalized procaine peaks in the whole examined area. These findings, combined with the fact that the pain-conducting fibers (the target structure of procaine) are located in the viable epidermis, allow us to conclude that the use of POE-23-lauryl ether will result in a more effective anesthesia.

The corresponding permeation experiments revealed that the permeation rate of procaine was not influenced by the two penetration enhancers. By contrast, the conventional penetration experiment as well as the CRM method detected significant differences in the content and distribution of procaine within the skin samples. These results clearly prove that the permeation rates and enhancement ratios are not adequate parameters for assessing the penetration enhancement. This holds especially true for drugs that are intended for intradermal action. In this case, the permeation rate may not be predictive of the drug content in the skin. Second, it is proven that the results that are obtained from the proposed CRM method correlate remarkably well with those of conventional penetration experiments.

In the case of POE-23-lauryl ether, the permeation rate remained constant as the procaine content in the skin increased. The penetration enhancement by POE-ethers has been shown to occur via disruption of the stratum corneum lipid matrix and an increase in the water content of the skin proteins. As a result, the permeation parameters, such as permeation rate, partition coefficient, and diffusion coefficient, are altered.[50] Apparently, POE-23-lauryl ether did not affect the permeation rate of procaine but did enhance its solubility in the skin, i.e., it enhanced the partition coefficient (skin/vehicle). This is fully in line with the calculated partition coefficients, which are significantly higher when procaine permeated from the formulation with POE-23-lauryl ether. The influence of POE-23-lauryl ether on the penetration and permeation of procaine is interesting, as it can be concluded that POE-23-lauryl ether will enhance the efficacy of procaine in the skin but will not lead to a higher systemic absorption.

5 Conclusion

The methods that have been proposed so far for the investigation of drug delivery to the skin by CRM are based on the acquisition of virtual cross-sections. These methods suffer from signal attenuation; thus, Raman signals can only be obtained from up to 40 μm below the skin surface.[21,24,25,44] By contrast, the proposed methodology allows an area corresponding to a depth of 70 μm inside the skin to be mapped by employing CRM on *ex vivo* cross-sections of skin. Deeper tissues could also have been mapped as no signal attenuation occurs. By mapping an area (image scan) in the skin instead of acquiring spectra along a line (line scan) perpendicular to the skin surface, the microstructure of the skin can be assessed. Our experiments show, in accordance with the findings of other groups, that the structure of the skin is not homogenous. Regions of high lipid content may be distinguished from regions of high protein and high water content.[21,22]

Therefore, it is reasonable to assume that APIs will not be distributed homogeneously across the skin depth. Our findings prove this assumption. The image of the skin sample penetrated by procaine from the formulation containing POE-23-lauryl ether shows particularly clearly that procaine is located in areas of high lipid content. This observation could not have been made via the sole acquisition of spectra along a line (line scan). Furthermore, the acquisition of a Raman scan in the image plane results in higher resolution compared to a virtual cross-section due to the loss in resolution that is caused by refraction, which increases with increasing depth in the sample.[42] As a result, the location of drugs in the skin and their co-location with skin contents can be mapped with higher precision in *ex vivo* skin samples. Thus, the proposed methodology allows the visualization of the drug distribution relative to the microstructure of the skin, allowing the examination of penetration pathways.

The increased depth accessible using *ex vivo* cross-sections as well as the acquisition of image scans are clear advantages of our methodology, as more detailed information can be obtained. However, our methodology relies on the use of *ex vivo* skin samples and is, therefore, not applicable for *in vivo* measurements.

One major challenge for future research will be the "real" quantification of the API in the skin. Apart from the concentration of the substance under investigation, the Raman signal is also influenced by matrix effects, e.g., by the matrix's refractive index and by signal attenuation due to refraction. To address this issue, the skin has conventionally been used as an internal standard in semiquantitative analyses of the drug content in the skin. This means that the peaks of APIs have been normalized to the so-called keratin signal (2910 to 2965 cm^{-1}) to render quantification possible.[20,24,25] We also normalized the procaine to this end. As outlined above, the structure of the skin is not homogenous, and any normalization has to be performed very carefully. The most challenging aspect of such further study will, therefore, be to enable the independent quantification of the API. Nevertheless, the authors believe that this quantification can be realized in the foreseeable future and that the proposed method will give more reliable results, as it is influenced by fewer parameters than virtual cross sections.

Appendix

This appendix gives further information on the data treatment in the course of the CRM evaluation and gives supplementary information on the impact of the penetration enhancers on CRM detection and quantification of procaine.

Figure 10 gives an illustration of the method that was applied to identify the spectrum with the highest intensity in the skin samples.

To preclude that the excipients of the formulations interfere with the detection of procaine in the skin and to evaluate if they can be detected in the skin, skin samples were incubated with placebo formulations. These were prepared as described in Sec. 2.2 with the only difference that no procaine HCl was added. Skin incubation and sample preparation followed the same regimen as for the formulations with API. Figures 11–13 show that no traces of the excipients were found in the skin. Furthermore, no peak at 1600 to 1625 cm^{-1} was found in the spectra of the excipients or the skin that had been incubated with the placebo formulations which could have interfered with procaine detection and (semi-)quantification.

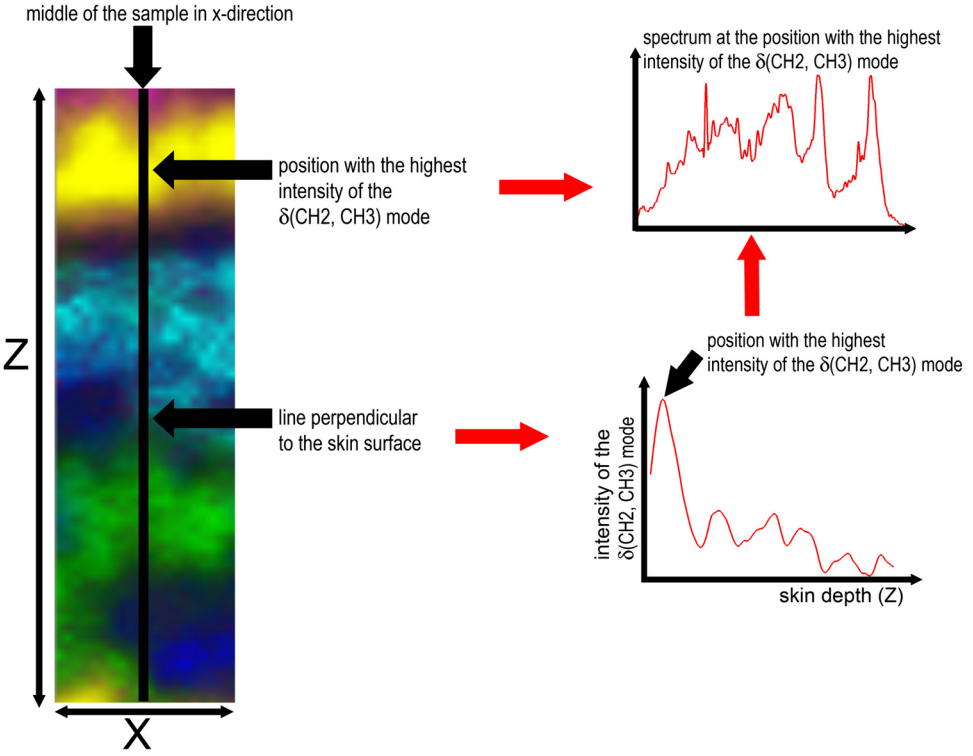

Fig. 10 Illustration of the procedure to extract the spectrum at the position with the highest spectral intensity.

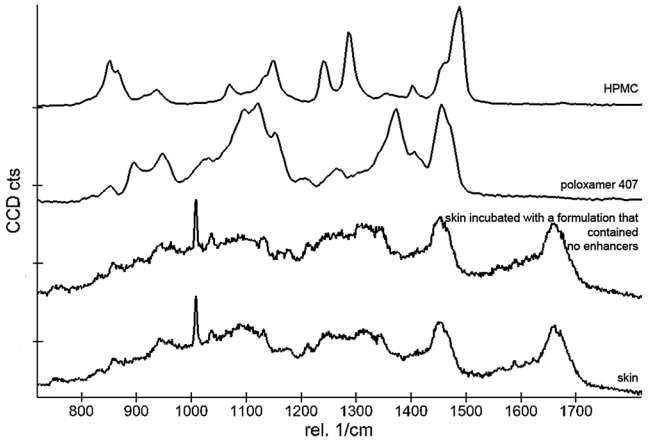

Fig. 11 Comparison of the CRM-spectra of the ingredients of the placebo formulation without enhancer, the skin and skin incubated with this formulation.

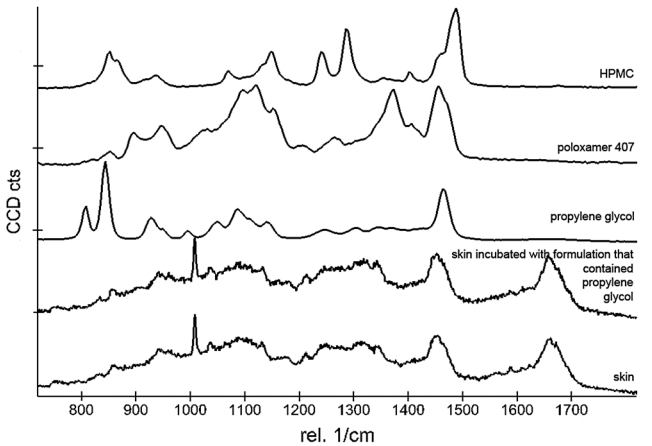

Fig. 12 Comparison of the CRM-spectra of the ingredients of the placebo formulation with propylene glycol, the skin and skin incubated with this formulation.

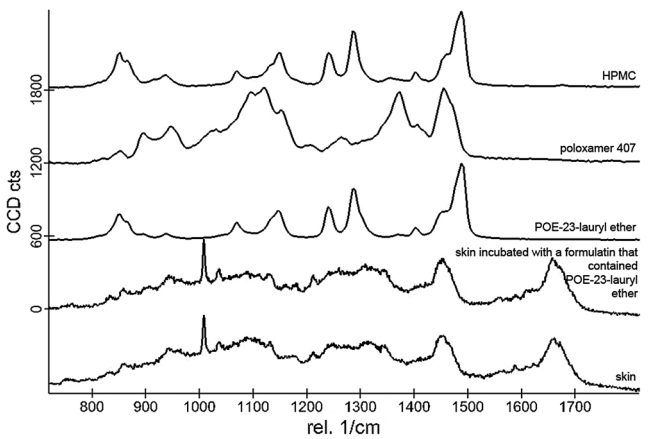

Fig. 13 Comparison of the CRM-spectra of the ingredients of the placebo formulation with POE-23-lauryl ether, the skin and skin incubated with this formulation.

Acknowledgments

The authors would like to thank Martin Schenk and his team from the Department of Experimental Medicine at the University of Tuebingen for the supply of pig ears.

References

1. P. M. Elias, "Epidermal lipids, barrier function, and desquamation," *J. Investig. Dermatol.* **80**(1), 44–49 (1983).
2. J. van Smeden et al., "The important role of stratum corneum lipids for the cutaneous barrier function," *Biochimica et Biophysica Acta* **1841**(3), 295–313 (2014).
3. R. O. Potts and R. H. Guy, "Predicting skin permeability," *Pharm. Res.* **9**(5), 663–669 (1992).
4. L. M. Russell and R. H. Guy, "Measurement and prediction of the rate and extent of drug delivery into and through the skin," *Expert Opin. Drug Deliv.* **6**(4), 355–369 (2009).
5. M. Bach and B. C. Lippold, "Percutaneous penetration enhancement and its quantification," *Eur. J. Pharm. Biopharm.* **46**, 1–13 (1998).
6. J. Hadgraft, "Skin, the final frontier," *Int. J. Pharm.* **224**(1–2), 1–18 (2001).
7. C. Valenta and B. G. Auner, "The use of polymers for dermal and transdermal delivery," *Eur. J. Pharm. Biopharm.* **58**(2), 279–289 (2004).
8. R. H. H. Neubert, "Potentials of new nanocarriers for dermal and transdermal drug delivery," *Eur. J. Pharm. Biopharm.* **77**(1), 1–2 (2011).
9. G. Cevc, U. Vierl, and S. Mazgareanu, "Functional characterisation of novel analgesic product based on self-regulating drug carriers," *Int. J. Pharm.* **360**(1–2), 18–28 (2008).
10. J. Brewer et al., "Spatially resolved two-color diffusion measurements in human skin applied to transdermal liposome penetration," *J. Investig. Dermatol.* **133**(5), 1260–1268 (2012).
11. E. Touitou, V. M. Meidan, and E. Horwitz, "Methods for quantitative determination of drug localized in the skin," *J. Controlled Release* **56**(1–3), 7–21 (1998).
12. R. Alvarez-Román et al., "Visualization of skin penetration using confocal laser scanning microscopy," *Eur. J. Pharm. Biopharm.* **58**(2), 301–316 (2004).
13. R. Mendelsohn, C. R. Flach, and D. J. Moore, "Determination of molecular conformation and permeation in skin via IR spectroscopy, microscopy, and imaging," *Biochim. Biophys. Acta* **1758**(7), 923–933 (2006).
14. B. Gotter, W. Faubel, and R. H. H. Neubert, "Optical methods for measurements of skin penetration," *Skin Pharmacol. Physiol.* **21**(3), 156–165 (2008).
15. W. Akhtar and H. G. M. Edwards, "Fourier-transform Raman spectroscopy of mammalian and avian keratotic biopolymers," *Spectrochim. Acta A* **53**(1), 81–90 (1997).
16. M. Gniadecka et al., "Structure of water, proteins, and lipids in intact human skin, hair, and nail," *J. Investig. Dermatol.* **110**(4), 393–398 (1998).
17. S. Wartewig et al., "Structure of stratum corneum lipids characterized by FT-Raman spectroscopy and DSC. IV. Mixtures of ceramides and oleic acid," *Chem. Phys. Lipids* **91**(2), 145–152 (1998).
18. C. Albèr et al., "Effects of water gradients and use of urea on skin ultrastructure evaluated by confocal Raman microspectroscopy," *Biochim. Biophys. Acta* **1828**(11), 2470–2478 (2013).
19. V. Wascotte et al., "Assessment of the "skin reservoir" of urea by confocal Raman microspectroscopy and reverse iontophoresis," *Pharm. Res.* **24**(10), 1897–1901 (2007).
20. P. J. Caspers et al., "*In vivo* confocal raman microspectroscopy of the skin: noninvasive determination of molecular concentration profiles," *J. Investig. Dermatol.* **116**(3), 434–442 (2001).
21. M. Ashtikar et al., "Non-invasive depth profile imaging of the stratum corneum using confocal Raman microscopy: first insights into the method," *Eur. J. Pharm. Sci.* **50**(5), 601–608 (2013).
22. F. D. Fleischli, S. Mathes, and C. Adlhart, "Label free non-invasive imaging of topically applied actives in reconstructed human epidermis by confocal Raman spectroscopy," *Vib. Spectrosc.* **68**(0), 29–33 (2013).
23. L. Franzen et al., "Towards drug quantification in human skin with confocal Raman microscopy," *Eur. J. Pharm. Biopharm.* **84**(2), 437–444.

24. R. Mateus et al., "A new paradigm in dermatopharmacokinetics—Confocal Raman spectroscopy," *Int. J. Pharm.* **444**(1–2), 106–108 (2013).
25. P. D. A. Pudney et al., "An *in vivo* confocal Raman study of the delivery of trans-retinol to the skin," *Appl. Spectrosc.* **61**(8), 804–811 (2007).
26. M. Förster et al., "Ingredients tracking of cosmetic formulations in the skin: a confocal raman microscopy investigation," *Pharm. Res.* **28**(4), 858–872 (2011).
27. J. Lademann et al., "*In vivo* Raman spectroscopy detects increased epidermal antioxidative potential with topically applied carotenoids," *Laser Phys. Lett.* **6**(1), 76–79 (2009).
28. A. Tfayli et al., "Follow-up of drug permeation through excised human skin with confocal Raman microspectroscopy," *Eur. Biophys. J.* **36**(8), 1049–1058 (2007).
29. C. Xiao et al., "Permeation of dimyristoylphosphatidylcholine into skin–Structural and spatial information from IR and Raman microscopic imaging," *Vib. Spectrosc.* **38**(1–2), 151–158 (2005).
30. C. Xiao et al., "Feasibility of tracking phospholipid permeation into skin using infrared and Raman microscopic imaging," *J. Investig. Dermatol.* **124**(3), 622–632 (2005).
31. G. N. Stamatas et al., "Lipid uptake and skin occlusion following topical application of oils on adult and infant skin," *J. Dermatol. Sci.* **50**(2), 135–142 (2008).
32. G. Zhang et al., "Imaging the prodrug-to-drug transformation of a 5-fluorouracil derivative in skin by confocal Raman microscopy," *J. Investig. Dermatol.* **127**(5), 1205–1209 (2007).
33. A. N. C. Anigbogu et al., "Fourier transform Raman spectroscopy of interactions between the penetration enhancer dimethyl sulfoxide and human stratum corneum," *Int. J. Pharm.* **125**(2), 265–282 (1995).
34. M. Gąsior-Głogowska et al., "FT-Raman spectroscopic study of human skin subjected to uniaxial stress," *J. Mech. Behav. Biomed. Mater.* **18**, 240–252 (2013).
35. P. J. Caspers et al., "Automated depth-scanning confocal Raman microspectrometer for rapid *in vivo* determination of water concentration profiles in human skin," *J. Raman Spectrosc.* **31**(8–9), 813–818 (2000).
36. G. R. Strichartz and B. G. Covinoin *Anaesthesia*, 3rd ed., R. D. Miller, Ed., p. 440, Churchill Livingstone Inc. (1990).
37. B. Bendas, U. Schmalfuβ, and R. Neubert, "Influence of propylene glycol as cosolvent on mechanisms of drug transport from hydrogels," *Int. J. Pharm.* **116**(1), 19–30 (1995).
38. B. W. Barry, "Modern methods of promoting drug absorption through the skin," *Mol. Aspects Med.* **12**(3), 195–241 (1991).
39. E. Squillante et al., "Codiffusion of propylene glycol and dimethyl isosorbide in hairless mouse skin," *Eur. J. Pharm. Biopharm.* **46**(3), 265–271 (1998).
40. F. P. Bonina and L. Montenegro, "Penetration enhancer effects on in vitro percutaneous absorption of heparin sodium salt," *Int. J. Pharm.* **82**(3), 171–177 (1992).
41. S.-C. Shin, C.-W. Cho, and K.-H. Yang, "Development of lidocaine gels for enhanced anesthetic action," *Int. J. Pharm.* **287**, 73–78 (2004).
42. N. J. Everall, "Confocal Raman microscopy: why the depth resolution and spatial accuracy can be much worse than you think," *Appl. Spectrosc.* **54**(10), 1515–1520 (2000).
43. WiTec Project data evaluation software user manual: Chapter 7 Data analysis, p. 70, WiTec Wissenschaftliche Instrumente und Technologie GmbH, D-Ulm (2008).
44. M. Mélot et al., "Studying the effectiveness of penetration enhancers to deliver retinol through the stratum cornum by *in vivo* confocal Raman spectroscopy," *J. Controlled Release* **138**(1), 32–39 (2009).
45. L. Franzen et al., "Advanced chemical imaging and comparison of human and porcine hair follicles for drug delivery by confocal Raman microscopy," *J. Biomed. Opt.* **18**(6), 061210 (2013).
46. European Medicines Agency, "ICH Topic Q 2 (R1) Validation of Analytical Procedures: Text and Methodology," (2005).
47. S. M. Ali et al., "Raman spectroscopic analysis of human skin tissue sections ex-vivo: evaluation of the effects of tissue processing and dewaxing," *J. Biomed. Opt.* **18**(6), 061202 (2013).
48. P. A. Bowser and R. J. White, "Isolation, barrier properties and lipid analysis of stratum compactum, a discrete region of the stratum corneum," *Br. J. Dermatol.* **112**(1), 1–14 (1985).
49. M. A. Palafox, "Raman spectrum of procaine hydrochloride," *Spectrosc. Lett.* **30**(6), 975–998 (1997).
50. E.-S. Park et al., "Enhancing effect of polyoxyethylene alkyl ethers on the skin permeation of ibuprofen," *Int. J. Pharm.* **209**(1–2), 109–119 (2000).

Dominique Jasmin Lunter is a postdoctoral fellow at the University of Tuebingen, Germany. She studied pharmacy at the University of Tuebingen and received a PhD in pharmaceutical technology from the same university.

Rolf Daniels is professor and head of the Department of Pharmaceutical Technology at the University of Tübingen, Germany. He studied pharmacy at the University of Regensburg (Germany) and received a PhD in pharmaceutical technology from the same university. Then he worked in the pharmaceutical development department of Pfizer (Illertissen) and was a postdoctoral fellow at the University of Regensburg before he completed his "Habilitation" thesis. He was appointed as full professor at the University of Braunschweig (1995–2005) before he moved to his current position.